Sensors and Actuators A 282 (2018) 55–62

Contents lists available at ScienceDirect

Sensors and Actuators A: Physical

journal homepage: www.elsevier.com/locate/sna

Optical, morphological and electrical analysis of heterostructures PSi/c-Si and SiO_2/MWCNTs/PSi/c-Si

N. Victoriano Huerta [a], J.A. Luna López [a,*], J.A.D. Hernández de la Luz [a], E. Gómez Barojas [a], A. Benitez Lara [b], K. Monfil Leyva [a], M.A. Domínguez Jimenez [a]

[a] CIDS-IC Benemérita Universidad Autónoma de Puebla, Ed. IC5 o IC6, Col. San Manuel, C.P. 72570 Puebla, Pue, Mexico
[b] Centro de Investigaciones en Óptica, Edif. H-1310, Loma del Bosque 115, Col. Lomas del Campestre, Código Postal 37150, León, Gto, Mexico

ARTICLE INFO

Article history:
Received 13 January 2018
Received in revised form 6 September 2018
Accepted 10 September 2018
Available online 12 September 2018

Keywords:
Porous silicon
MWCNTs
Photoluminescence
SEM
Morphology
Electrical characterization

ABSTRACT

Porous silicon (PSi) has been studied extensively due to its photo luminescence (PL) in the visible range at room temperature. PSi layers are useful for various optical and electrical applications among others. The PSi properties can be enhanced using different materials. In the present work, we have decorated PSi single layers with multiple wall carbon nanotubes (MWCNTs). The thickness of PSi layers was determined by the gravimetric analysis, the surface morphology by scanning electron microscopy (SEM), the optical properties were studied by measuring PL and reflectance spectra and the electrical behavior was analyzed from the measured I–V curves for which some theoretical transport mechanisms are used to make a study in depth. These materials and structures have potential applications in chemical sensors.

1. Introduction

In 1956 the PSi was discovered by Uhlir, however such fact was unnoticed. It was until the 70 s and 80 s decades that this material became important being used in chemical sensors applications. In 1990 Leigh Canham discovered the PL of PSi at room temperature [1], this event stumped the scientific community in such a way that a cascade of research works about its PL properties and simultaneous applications based on PSi multilayers such as sensors, dielectric Bragg reflectors and so on [2–4].

Diverse works have reported outstanding modifications in the original properties of porous silicon when infiltrated with different materials forming in general hybrid systems, in such materials may be included the carbon nanotubes (CNTs). Nowadays CNTs, in the form of either single-walled carbon nanotubes (SWCNTs) or multi-walled carbon nanotubes (MWCNTs) [5–7], are one dimensional systems in nature and present unique physical and chemical properties and their prospects for practical applications, besides they may be either semiconducting or metallic systems. Apart from these characteristics, they exhibit diverse properties such as low resistivity and high electrical conductivity, and a few nanometers in diameter, among others. The CNTs are usually used to improve the properties of different materials [8]. Today, there are various techniques for growing CNTs, the methods commonly used are arc discharge, laser ablation, chemical vapor deposition and electrolysis [9]. There is a great interest to grow CNTs using various materials, mainly silicon substrates since this material is widely used for building electrical and optical devices. Along the last century have been used techniques such as chemical vapor deposition [10–15], spray pyrolysis [16–21], among others to grow CNTs in different materials, however such techniques necessarily use high cost reactors being this latter a drawback so as an advantageous alternative it is possible to build hybrid systems by using the deposition of CNTs on the material by the spin coating method.

The properties of MWCNTs make them for use in chemical sensing application, such as gas sensor, biosensor, etc. [22–27]. The sensitive, fast response and stability are advantages of gas sensor based in CNTs [22,27], they also show susceptibility with molecules of NO_2 [23], explosive gases, vapor-sensitive polymers, semiconductor metal oxides, etc. [28–35]. Considering the relevant importance of the hybrid systems using CNTs to improve optical and electrical properties and their potential applications in the field of novel devices. In the present work heterostructures of type PSi/c-Si and SiO_2/MWCNTs/PSi/c-Si have been synthesized and their morphological, optical and electrical properties have been analyzed.

* Corresponding author.
E-mail address: jose.luna@correo.buap.mx (J.A. Luna López).

https://doi.org/10.1016/j.sna.2018.09.030
0924-4247/

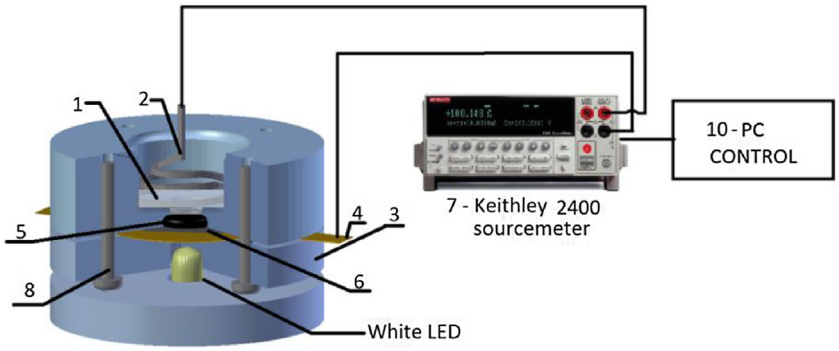

Fig. 1. Schematic diagram of electrochemical cell: 1 - electrolyte or anodic solution, 2 - cathode of tungsten, 3 - electrochemical cell (Teflon), 4 - anode of nickel, 5 - seal (O-ring), 6 - wafer of c-Si, 7 - Keithley 2400 source-meter, 8 - screws, 9 - Light source (white LED), 10 - PC control.

2. Experimental methods

PSi single layers were synthesized on Si n-type substrates with orientation <100> and low resistivity (<0.005 Ω·cm) by electrochemical anodization using a Teflon cell. The electrochemical system setup is shown in Fig. 1. The etching solution contained $C_2H_6O : HF : C_3H_8O_3$ in volume with a proportion: 6:3:1, with anodization current densities of 7.5 $\boldsymbol{mA/cm^2}$, 37.6 $\boldsymbol{mA/cm^2}$ and (c) 75.35$\boldsymbol{mA/cm^2}$, applied on an area of 1.32 cm^2. A white LED was used as an illumination source to photo-generate the necessary holes for the formation of pores, the procedure was carried out in the dark to avoid undesirable light [3]. The light illuminated only the rear side of the silicon wafer, Fig. 1 shows the experimental home-built setup.

The type of MWCNTs utilized in this works are described by Hordy et al. [21], such MWCNTs were obtained using chemical vapor deposition, directly from stainless steel 316 mesh, without any pretreatment or the use of an external catalyst. For the present work the mesh with MWCNTs was dissolved in 500 ml of Ethanol-Reagent-Grade 99.9% per vol. adding 0.1% of Triton 100 x by sonication. For dispersion of MWCNTs on the PSi single layers, 10 drops of 0.05 ml of solution was spun starting from 3000 rpm for 15 s and increasing the spinning speed up to 5000 rpm; this process was repeated 5 times since previous investigations confirm that much greater presence of CNTs reduces the sheet resistance of the single layers [37]. To determine the size and distribution of the MWCNTs in MWCNT/ethanol solutions, a Nano-ZS90, Zetazizer Software was used using dynamic light scattering at a dispersion angle of 90 degrees under normal conditions, T = 25 °C. For the MWCNT, the refractive index of 2.47 and an absorption coefficient of 0.99 were considered, and for the dispersing material (ethanol) a refractive index of 1359 and a viscosity of 14.20 cp. It was determined that a volume of 6.2 ml the MWCNT/ethanol solution contained in a glass tube contains only MWCNTs with a length of 726 nm. The mass of MWCNTs dispersed in the solution is 0.01116 g, forming a solution whose density is 0.775 g/ml. The concentration of MWCNTs in solution is 1.8 g/l. Therefore, 10 drops of the MWCNT/ethanol solution contain only MWCNTs with a length of 726 nm. The mass of MWCNTs dispersed in 10 drops (.5 ml) is 0.0009 g, forming a solution whose density is 0.7755 g/ml, and the concentration of MWCNTs in solution is 1.8 g/l. After deposition of MWCNTs, the samples were thermally oxidized in a tubular furnace at T = 300 °C in an environment of 10 ml/min of O_2 flow for 5 min. Santamaría-Juárez et al. [38] have shown that the optical properties of PSi thermally oxidized at 300 °C for 5 min, are less attenuated than those for longer times. The oxidation process generates chemical bonds in such a way that the MWCNTs are better anchored to the PSi layers. Finally, under these conditions we were able to build a heterostructure of the type SiO_2/CNT/PSi/c-Si.

Table 1
List of etching conditions and pore parameters of the heterostructures SiO_2/MWCNTs/PSi/c-Si. Analysis data obtained from SEM micrographs.

Sample	Anodizing current density	Pore width (nm)	Distance between pores (nm)
PSCNTM1	7.5 $\boldsymbol{mA/cm^2}$	30 a 45	50 a 112
PSCNTM2	37.6 $\boldsymbol{mA/cm^2}$	40 a 60	70 a 80
PSCNTM3	75.35 $\boldsymbol{mA/cm^2}$	105 a 275	30 a 50

3. Results and discussion

The porosity and thickness of the PSi layers were determined by the gravimetric method using the formula $\%P = \frac{m_1 - m_2}{m_1 - m_3}$, where m_1 is the weight of the sample before the PSi is grown, m_2 is the weight after the PSi layer has been grown and m_3 the weight after the PSi layer has been removed [39,40]. The PSi layer thickness was determined using the equation $d = \frac{m_1 - m_3}{S * \rho}$, where in our case the PSi grown area is 1.23 cm^2, and $\rho = 2328 \frac{mg}{cm^3}$ is the silicon density [39]. The Fig. 2a shows a plot of PSi layer thickness vs. etching time and (b) is a plot of porosity percentage vs. etching time. The latter is not linear. In (a) it is observed that keeping constant the anodizing current, the PSi layer thickness increases for greater etching times where in general the greater anodizing current the greater layer thickness, existing limited regions where the behavior is linear, while in (b) the porosity exhibits an increment when increasing the anodizing current but linear behavior is almost absent.

On the other hand, porosity and etching rate versus anodizing current, for a fixed anodized time of 10 min, is plotted in Fig. 3. In Fig. 3 (a) is observed that as the current increases so does the porosity. In addition in Fig. 3 (b), the etching rate is calculated as $r = d/t$ where d is the thickness of the PSi layer and t the process time, and the etching rate displays a tendency to increase linearly.

The characterizations were performed at room temperature; the morphology of the samples was characterized by using a scanning electron microscope (SEM) Hitachi model SU3500. Several investigations confirm that the porosity of a PSi layer increases as the current density is increased and that at a fixed current density, the thickness of a layer increases as the processing time is increased [12]. Fig. 4 shows SEM micrographs of the surface morphology of the samples. It can be seen that increasing the anodizing current, the porosity percentage of the PSi layers is increased. Additionally, from this figure it is observed the presence of the MWCNTs so that the deposition of MWCNTs on the surface of the PSi layers was successful.

In Table 1, the width and average pore diameters are listed; these results were obtained with SPIP software. According to these data different pore sizes were obtained, namely: mesopores are obtained for an anodization current density of 7.5 $\boldsymbol{mA/cm^2}$, macropores for 37.6 $\boldsymbol{mA/cm^2}$ and macropores for 75.35 $\frac{\boldsymbol{mA}}{\boldsymbol{cm^2}}$.

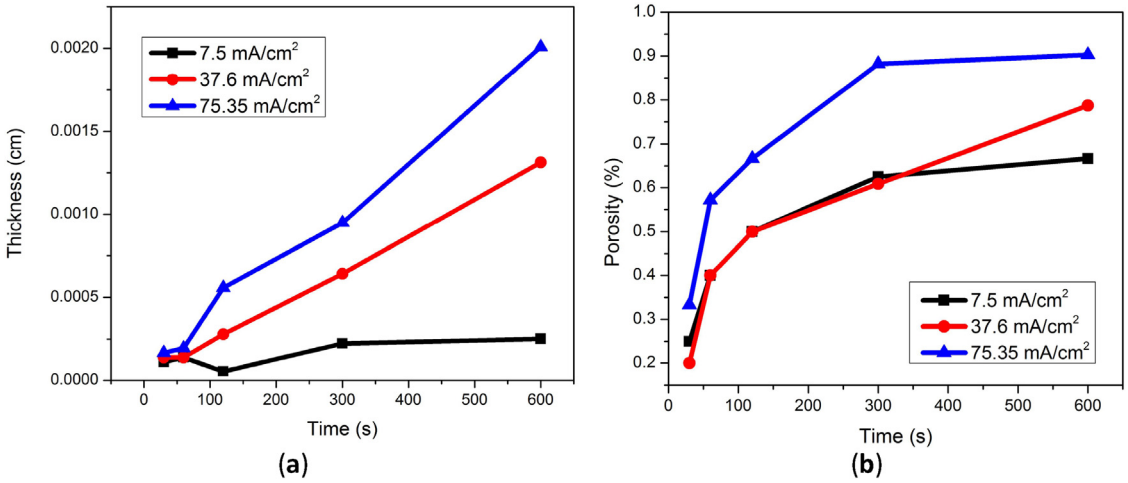

Fig. 2. (a) Thickness vs. etching time of PSi single layers at different anodization currents and (b) Porosity vs. etching time at the same different anodization currents.

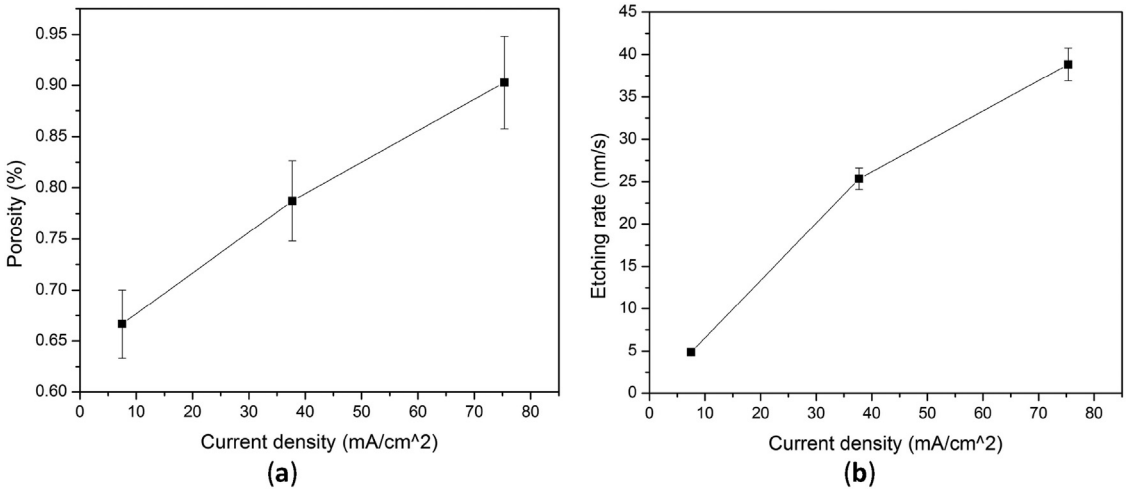

Fig. 3. (a) Plot of P% of PSi layers obtained at different current densities and constant anodization time and (b) is a plot of Etching rate vs Current Density.

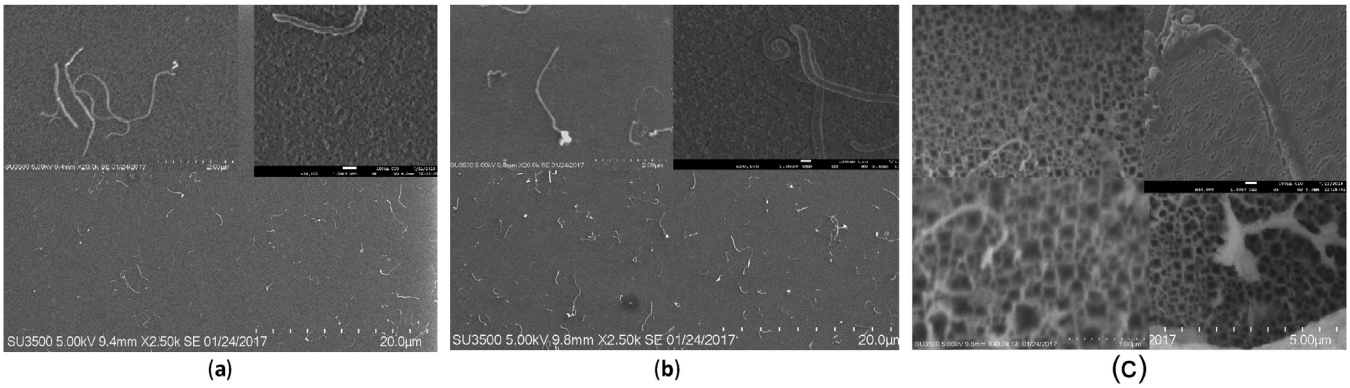

Fig. 4. SEM micrographs of surface morphology of heterostructures SiO_2/MWCNTs/PSi/c-Si obtained with anodization current densities: (a) 7.5 $\boldsymbol{mA/cm^2}$ for 10 min, (b) 37.6 $\boldsymbol{mA/cm^2}$ for 10 min and (c) 75.35 $\boldsymbol{mA/cm^2}$ for 10 min. All insets show a nanotube in PSi, the scale is at 100 nm.

The diffuse reflectance spectra were obtained with a spectrophotometer UV-VIS-NIR Agilent Cary, 5000 series, with a sweep from 200 to 800 nm, at different angles from 20° to 70°, and the graphs with more information were selected, being those that were measured at 60°. In Fig. 5 the reflectance spectra of the PSi single layers and SiO_2/MWCNTs/PSi/c-Si structures are shown. In (a) the spectra correspond to PSi layers obtained at 7.5 $\boldsymbol{mA/cm^2}$ of anodizing current for different etching times, labeled as PSM1(A), PSM1(B) and PSM1(C). In (b) the spectra correspond to PSi layers with CNTs obtained at 7.5 $\boldsymbol{mA/cm^2}$ of anodizing current for different etching times, labeled as PSCNTM1(A), PSCNTM1(B) and PSCNTM1(C). The Fabry-Perot oscillations exhibited in these spectra are due to the effect of the different PSi layer thicknesses [13–16].

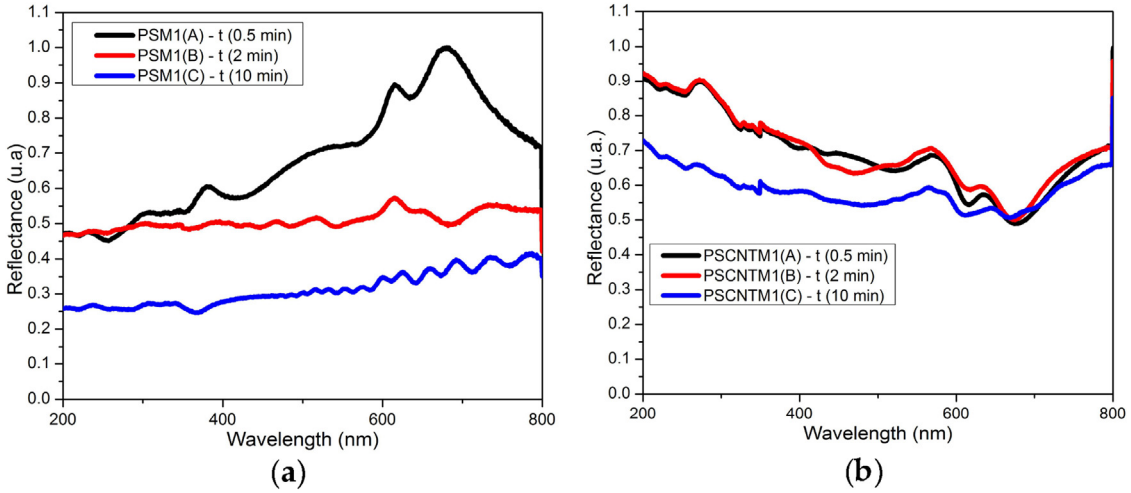

Fig. 5. Reflectance spectra of heterostructures (a) PSi/c-Si, (b) SiO_2/MWCNTs/PSi/c-Si, obtained with 7.5 mA/cm^2.

As has been mentioned above, the porosity depends strongly on the anodization time thereby the PSi surface area suffers important changes on its topology when the time parameter is increased such fact generates essential changes in the light dispersion so when the pores density increases the effect of light confinement provoked by the pores which enhance the reflectivity diminishes substantially for this reason we observe the lowest reflectance in (a) for 10 min anodization time. On the other hand, in (b) the presence of SiO_2 acting as a coating layer modifying the influence of the pores and the MWCNTs anchored on the surface area, both modify drastically not only the structure of the reflectance spectra but also the intensity, particularly in the region of 400–750 nm, the decreasing of the reflectance spectra may be caused by the surface of PSi layers coated by the MWCNTs whose dispersion generates light trapping.

The photoluminescence spectra were obtained with a Horiba Jobin Yvon spectrofluorometer, model Fluoromax-3, using a beam of light with an excitation length of 252 nm, a bandpass filter with a wavelength of 300 nm, scanning from 370 nm to 1000 nm, keeping slits at 3 nm aperture. The photoluminescence spectra shown in Fig. 6 (a) were obtained from PSi layers without MWCNTs. Mainly two PL bands are observed, one lies in the range approximately of 400–500 nm whose maximum is about at 430 nm and other wide band in the range of 500–900 nm. The latter exhibits a shoulder which is noticeable at about 840 nm. The second band placed in the region of lower energies changes its structure (width and height) when anodization time increases which means that the pore density and pore size play a key role in the optical response of the material. In this case, the two bands have a high intensity and a big wide band, if they are compared with Fig. 6(b), where the MWCNT/PSi samples have a peak blue more notable, and for cases of 0.5 and 2 min the red peak does not appear. These are some outstanding differences which are very notable from the samples with and without MWCNTś.

Fig. 6 shows the PL of the same samples shown in Fig. 5, the marking is the same because the samples have the same growth process. Fig. 6 (b) shows the photoluminescence spectra of PSi layers decorated with MWCNTs and with additional thermal oxidation performed after the MWCNT deposition. The MWCNT coverage on PSi layers is determined by the conditions already mentioned above, i.e., only one value of MWCNT concentration was considered as well as the dispersion type, this was done in this way since our main interest is focused on observing the optical response of the MWCNTs-PSi structure. We observe that there is a clear tendency to form two main bands in the blue and red regions due to micro/nano hierarchical structure in porous silicon [45,46]. Predominantly, the

Table 2
Electrical properties values of monolayers of PSi.

Sample	Anodization current density	$J_s\,(A/cm^2)$	$\phi_b\,(eV)$	$R_S(\Omega)$	n
PSM1	7.5 mA/cm^2	8.56643E-10	0.731	584.443	72.904
PSM2	37.6 mA/cm^2	3.63464E-06	0.515	339.529	140.809
PSM3	75.35mA/cm^2	3.897E-04	0.394	962.000	23.571
PSCNTM1	7.5 mA/cm^2	15.585E-04	0.358	282.941	131.326
PSCNTM2	37.6 mA/cm^2	4.5095E-05	0.390	1018.069	21.247
PSCNTM3	75.35mA/cm^2	1.6538E-04	0.416	375.723	8.246

influence of the Si-O, SiH_x and Si−OH bonds determine the shape of the luminescence spectrum and to a lesser extent the influence of the creation of a hydrogen-carbon surface between the carbon atoms in the MWCNT and H-Si in the PSi layer [42–45].

In this work it was needed to study the electrical behavior of our heterostructures in order to analyze the charge transport phenomenon in this type of systems, for such aim we proceed to build aluminum contacts between 500 to 750 nm of thickness which were deposited by the sputtering technique, a mask with circles of 1 mm in diameter was used on top side. The J–V curves in Fig. 7 (a) are obtained from PSi monolayers with different anodization current densities as is listed in Table 2, while those in Fig. 7 (b) correspond to monolayers with MWCNTs, in both cases they have rectifying behavior. Several previous works explain that a Schottky barrier is formed at the metal/PSi interface, according to the work function of Al, an ohmic contact should be formed when the metal/PSi junction is performed, but we find that the electrical behavior is rectifying, such fact is attributed to the existence of a high density of surface states which are present on PSi surface area and are activated by the external electric field, their influence creates a barrier against the flow of current [19,20]. Therefore, some I–V curves have a behavior as Schottky barrier or SCLC (Space Charge Limited Current). An analysis of the current mechanism was realized with these I–V curves in order to determine its possible conduction mechanism as it is proposed in the following paragraphs.

The data of the I–V curves were analyzed considering that a Schottky barrier is built in such case we have the corresponding equations:

$$I = I_S\left\{\exp\left[\frac{qV_D}{nkT}\right] - 1\right\} \quad (1)$$

$$I_S = AA^*T^2\exp\left(-\frac{q\phi_B}{kT}\right) \quad (2)$$

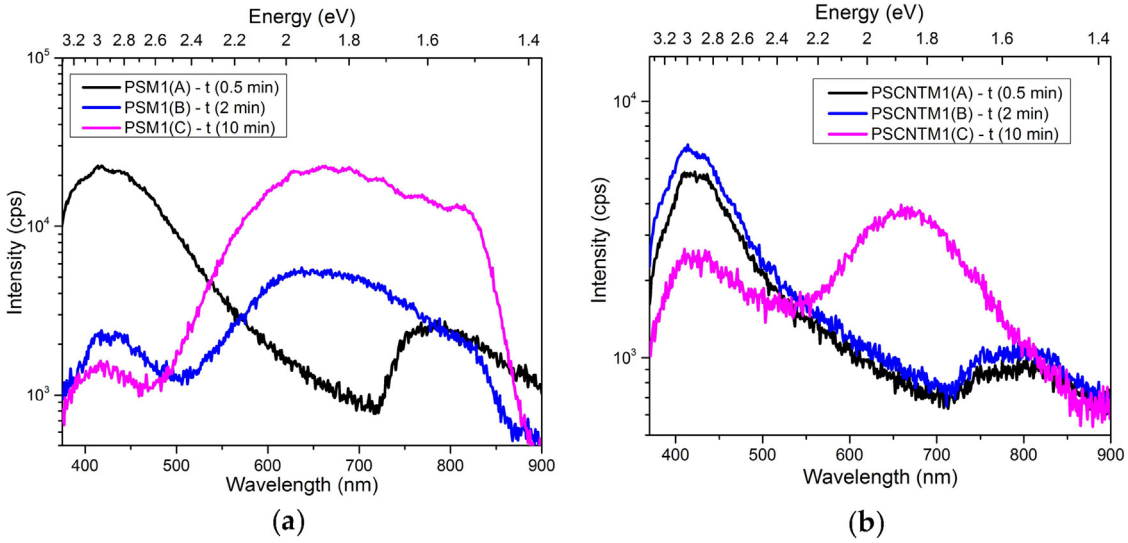

Fig. 6. Photoluminescence spectra of heterostructures (a) PSi/c-Si and (b) SiO_2/MWCNTs/PSi/c-Si, obtained at 7.5 $\boldsymbol{mA/cm^2}$ of anodization current density.

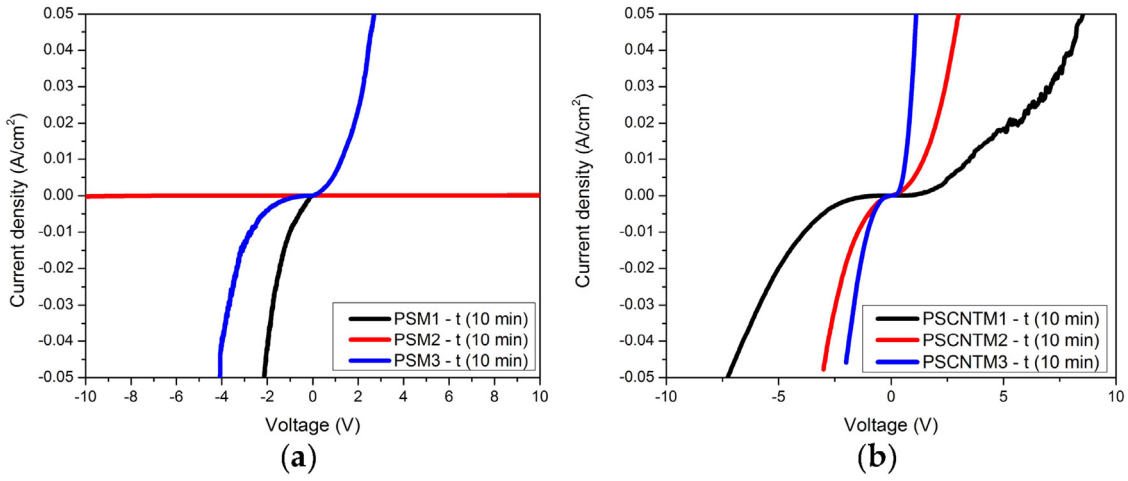

Fig. 7. J–V curves of heterostructures (a) PSi/c-Si, (b) SiO_2/MWCNTs/PSi/c-Si, with 7.5 $\boldsymbol{mA/cm^2}$, 37.6 $\boldsymbol{mA/cm^2}$ and 75.35 $\boldsymbol{mA/cm^2}$ of anodization current densities.

where V_D is the voltage applied through the Schottky barrier, n the ideality factor, k Boltzmann's constant, I_S is the saturation current or in terms of density current it is substituted by $J_s = I_S/A$, ϕ_B is the height of the Schottky barrier, T the temperature in kelvin, A is the effective area of the diode and $A^* \approx 112\,Acm^{-2}k^{-2}$ is Richardson's constant for c-Si type n [47].

The effect of the series resistance of a Schottky barrier is usually modeled with a combination of the barrier and a resistance R_s through which a current I flows, in terms of voltage V. Due to the combination of the barrier with the resistor, we have the expression $V_D = V - IR_s$, modifying the Eq. (1) to:

$$I = I_S\left\{\exp\left[\frac{q(V - IR_s)}{nkT}\right] - 1\right\} \tag{3}$$

To determine the parameters, the linear region given by the graph is required $\ln(I)\,vs\,V$ [45–50], where the point of intersection is I_S and the slope is $\frac{qV_D}{nkT}$, additionally to find R_s it is necessary to follow the Cheung and Cheung method [47,48], plotting $dV/d(\ln I)\,vs\,I$ and $H(V)\,vs\,I$, where:

$$\frac{dV}{d(\ln I)} = R_s I + nkT/q \tag{4}$$

$$H(I) = R_s I + n\phi_B, \tag{5}$$

From Eq. (4), R_s and n can be estimated and alike ϕ_B by Eq. (5). Table 2 shows the data obtained for the different samples anodized for 10 min.

The samples PSM1, PSM2 and PSM3 correspond to monolayers with PSi, the analysis shows that as the anodizing current is higher, J_S, ϕ_b is reduced and R_S is increased, while n has no a clear tendency in its behavior; this can be understood that as the thickness of the PSi monolayer increases, so does the resistance associated with it. The samples PSCNTM1, PSCNTM2 and PSCNTM3, which correspond to heterostructures Al/SiO_2/MWCNTs/PSi/c-Si/Al show that as the thickness of the PSi monolayer increases, J_S take values between 1.6538E-04 and 4.5095E-05 A/cm^2, ϕ_b and n decreases, while there is no clear trend for R_S, due to the deposition of MWCNTs, although the thickness influences significantly, so does the pore size in the PSi, because as the pore diameter is greater, there is a major probability that MWCNTs could be inserted into the pore and not only superficially, reducing the value of parameters in the Schottky barrier formed. Investigations of diverse heterostructures attributed to the gas sensing mechanism to Schottky barrier formation [17,49–53], Gusain, Abhay et al. [49] use a gas sensor based on a conducting polymer for sensing NO, Nguyen Minh Triet et al. [50] use heterojunction for sensing NO_2, SO_2, and HCHO, the investigations showed high sensivity, fast response, etc.

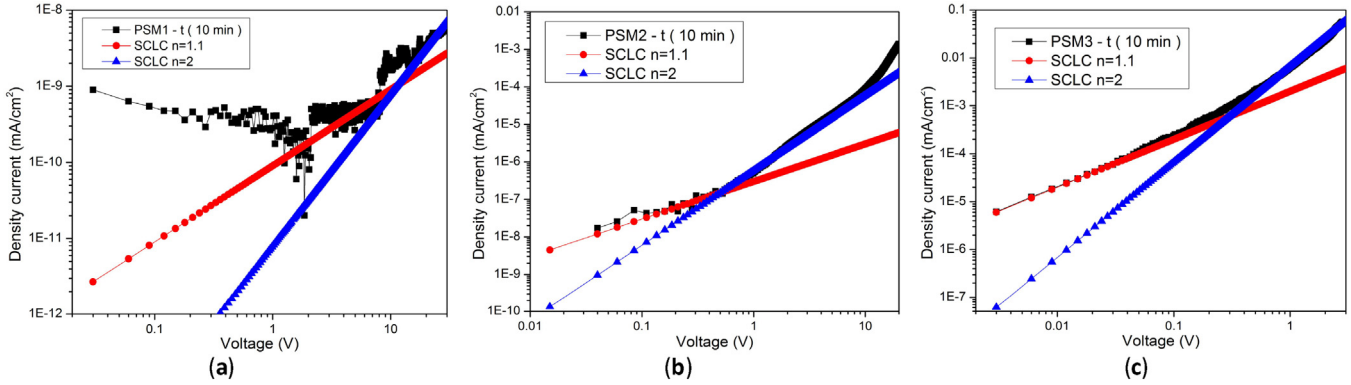

Fig. 8. Curves $\boldsymbol{log}\,(\boldsymbol{J})\,\boldsymbol{vslog}\,(\boldsymbol{V})$ practices and heterostructure transport mechanism PSi/c-Si with anodization current density of (a) $7.5\,\boldsymbol{mA/cm^2}$, (b) $37.6\,\boldsymbol{mA/cm^2}$ and (c) $75.35\boldsymbol{mA/cm^2}$, for 10 min.

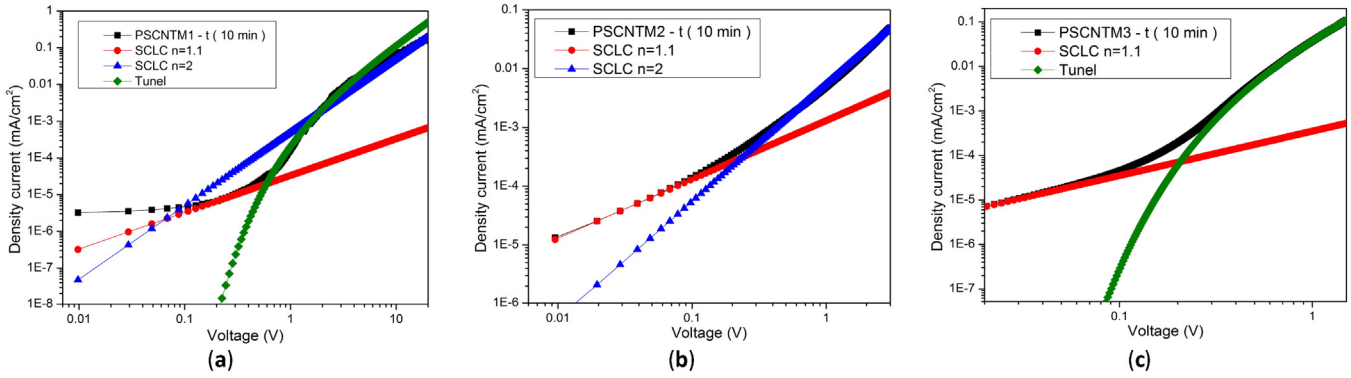

Fig. 9. Curves $\boldsymbol{log}\,(\boldsymbol{J})\,\boldsymbol{vslog}\,(\boldsymbol{V})$ practices and heterostructure transport mechanism SiO_2/MWCNTs/PSi/c-Si with anodization current density of (a) $7.5\,\boldsymbol{mA/cm^2}$, (b) $37.6\,\boldsymbol{mA/cm^2}$ and (c) $75.35\boldsymbol{mA/cm^2}$, for 10 min.

Additionally the transport mechanisms in the samples have been searched. The curves $\log(J)$ *vs* $\log(V)$ corresponding to the samples of PSi with anodization time of 10 min and anodization current density with values of $7.5\,\boldsymbol{mA/cm^2}$, $37.6\,\boldsymbol{mA/cm^2}$ and $75.35\boldsymbol{mA/cm^2}$ are presented in Fig. 8, the simulated load transport curve was added. The curves show a behavior $J \propto V^n$, corresponding to the SCLC transport mechanism with $n = 2$ as the predominant mechanism, this behavior has already been reported in different works [45,46,54,55], due to the fact that the current in the device is dominated by the transport of carriers in the PSi layer of high resistivity, which can be modeled as an interleaving between two conductive materials because the band in the metal/PSi interface is so small that the junction Schottky can be neglected; n values also have been found, with $n = 1.1$ or 2 at low voltages, (a behavior observed in various reports), when the current has a linear behavior [55].

Fig. 9 shows the curves $\log(I)$ *vs* $\log(V)$ for the SiO_2/MWCNTs/PSi/c-Si heterostructures obtained for 10 min of anodization time, all samples showed a SCLC transport mechanism with n = 1.1 for voltages in the vicinity of 0 V. For the samples at $7.5\,\boldsymbol{mA/cm^2}$ and $37.6\,\boldsymbol{mA/cm^2}$ of anodization current density, we have another region with SCLC transport but using n = 2. The voltage regions in which the current density behaves as $J \propto V^2 exp(-b/V)$, correspond to the Fowler-Nordheim mechanism where b is a coefficient related to the carrier effective mass and an energetic barrier height that the carriers need to across for an electrical conduction [55], this type of conduction mechanism is presented by samples at $7.5\,\boldsymbol{mA/cm^2}$ and $75.35\,\boldsymbol{mA/cm^2}$. This electrical behavior exhibited in our structures can be attributed to the contribution of the low dimensional MWCNTs which have showed this kind of transport mechanism [56–58].

The addition of MWCNTs to the monolayers of PSi, turns out to be a positive contribution, since the parameters of the formed Schottky barrier are optimized, decreasing the barrier height, the ideality constant and the resistance, while the transport mechanism is modified, showing a Tunneling Fowler-Nordheim behavior.

4. Conclusion

The monolayers of PSi/c-Si and SiO2/MWCNTs/PSi/c-Si take advantage of the various properties, because the gravimetric analysis shows that longer anodizing times result in greater thickness. SEM micrographs show that as the anodizing current is increased larger pores are obtained. The different pore sizes, provides selectivity for the interaction or confinement of molecules or low dimensional systems as MWCNTs all which produces outstanding effects in the electrical and optical properties of the heterostructures.

The photoluminescence spectra showed the appearance of two main bands placed in the UV region and other in the red region, this optical behavior can be used for optical gas sensors where the filling factor of different substances can be measured by using an interferometric technique. The I–V curves of the heterostructures PSi/c-Si and SiO2/MWCNTs/PSi/c-Si displayed an electrical rectifying behavior; such behavior is attributed to the Schottky barrier formation.

The transport mechanism found in the PSi-based heterostructures is of type SCLC, the most common in these systems, while for the PSi-based heterostructures with MWCNTs aggregated, exhibit Fowler-Nordheim tunneling, the transport mechanism which is suitable for the field emission tunneling devices encompassing gas sensors based on semiconducting nanowire Field-Effect tran-

sistors. The morphological, optical and electrical characterization have shown that the MWCNTs aggregated amplify the field of application of these heterostructures, especially to make up different gas sensors devices and the additional thermal treatment is expected to be useful for enlarging the life time of the PSi-based layers.

Author contributions

N.Victoriano Huerta and *J.* A. Luna López conceived and designed the experiments; N. Victoriano Huerta, and E Gómez Barojas performed the experiments; N. Victoriano Huerta, *J.* A. Luna López, K. Monfil Leyva, M. A. Dominguez Jimenez, A. Benitez Lara analyzed the data; N. Victoriano Huerta, *J.* A. D. Hernández de la Luz, E. Gómez Barojas and *J.* A. Luna López wrote the paper.

Conflicts of interest

"The authors declare no conflict of interest".

Acknowledgments

This work has been partially supported by CONACyT-CB-255062 and VIEP-LULJ-EXC-2018. The authors acknowledge CIDS, CIO, INAOE and IFUAP laboratories for their help in the samples characterizations. The authors are thankful to Dr. Norma Mendoza and the McGill Institute for supplying MWCNTs for the present work.

References

[1] S. Basu, J. Kanungo, Nanocrystalline porous silicon, in: S. Basu (Ed.), Crystalline Silicon - Properties and Uses, InTech, Croatia, 2011, pp. 219–235.
[2] J. Escorcia Garcia, O. Sarracino Martíinez, J.M. Gracia-Jiménez, V. Agarwal, Porous silicon photonic devices using pulsed anodic etching of lightly doped silicon, J. Phys. D 42 (2009) 145101, http://dx.doi.org/10.1088/0022-3727/42/14/145101.
[3] D.H. Ge, M.C. Wang, W.J. Liu, S. Qin, P.L. Yan, J.W. Jiao, Formation of macro-meso-microporous multilayer structures, Electrochim. Acta 88 (2013) 141–146, http://dx.doi.org/10.1016/j.electacta.2012.10.028.
[4] M. Ghulinyan, C.J. Oton, L.D. Negro, L. Pavesi, R. Sapienza, M. Colocci, D.S. Wiersma, Light-pulse propagation in fibonacci quasicrystals, Phys. Rev. B 71 (2005) 094204, http://dx.doi.org/10.1103/PhysRevB.71.094204.
[5] S. Iijima, Helical microtubules of graphitic carbon, Nature 354 (1991) 56–58, http://dx.doi.org/10.1038/354056a0.
[6] C. Chen, Y. Zhang, Nanowelded Carbon Nanotubes: From Field Effect Transistors to Solar Microcells. Nanosci. and Technol., Springer, Berlin, 2009, http://dx.doi.org/10.1007/978-3-642-01499-4.
[7] B.K. Kaushik, M.K. Majumder, Carbon Nanotube Based VLSI Interconnects: Analysis and Design, Springer, India, 2015, http://dx.doi.org/10.1007/978-81-322-2047-3_3.
[8] Carbon nanotube electronics, in: A. Javey, J. Kong (Eds.), Integrated Circuits and Systems, Springer, US, 2009, http://dx.doi.org/10.1007/978-0-387-69285-2.
[9] R. Purohit, K. Purohit, S. Rana, R.S. Rana, V. Patel, Carbon nanotubes and their growth methods, Procedia Mater. Sci. 6 (2014) 716–728, http://dx.doi.org/10.1016/j.mspro.2014.07.088.
[10] H.G. Shiraz, F.R. Astaraei, S. Fardindoost, Z.S. Hosseini, Decorated CNT based on porous silicon for hydrogen gas sensing at room temperature, RSC Adv. 50 (2016) 44410–44414, http://dx.doi.org/10.1039/C6RA03541H.
[11] J. Song, D.S. Jensen, D.N. Hutchison, B. Turner, T. Wood, A. Dadson, M.A. Vail, M.R. Linford, R.R. Vanfleet, R.C. Davis, carbon-nanotube-templated microfabrication of porous silicon-carbon materials with application to chemical separations, Adv. Funct. Mater. 21 (2011) 1132–1139, http://dx.doi.org/10.1002/adfm.201001851.
[12] W.D. Zhang, Y. Wen, W.C. Tjiu, G.Q. Xu, L.M. Gan, Growth of vertically aligned carbon-nanotube array on large area of quartz plates by chemical vapor deposition, Appl. Phys. A 74 (2002) 419–422, http://dx.doi.org/10.1007/s003390101187.
[13] Z.F. Ren, Z.P. Huang, J.W. Xu, J.H. Wang, P. Bush, M.P. Siegal, P.N. Provencio, Synthesis of large arrays of Well-aligned carbon nanotubes on glass, Science 282 (1998) 1105–1107, http://dx.doi.org/10.1126/science.282.5391.1105.
[14] H. Gammoudi, F. Belkhiria, K. Sahlaoui, W. Zaghdoudi, M. Daoudi, S. Helali, F. Morote, H. Saadaoui, M. Amlouk, G. Jonusauskas, T. Cohen-Bouhacina, R. Chtourou, Enhancement of the photoluminescence property of hybrid structures using single-walled carbon nanotubes/pyramidal porous silicon surface, J. Alloys Compd. 731 (2018) 978–984, http://dx.doi.org/10.1016/j.jallcom.2017.10.040.
[15] Z.W. Pan, S.S. Xie, B.H. Chang, C.Y. Wang, Y. Lu, W. Liu, W.Y. Zhou, W.Z. Li, L.X. Qian, Very long carbon nanotubes, Nature 394 (1998) 631–632, http://dx.doi.org/10.1038/29206.
[16] D. Xu, G. Guo, L. Gui, Y. Tang, Z. Shi, Z. Jin, Z. Gu, W. Liu, X. Li, G. Zhang, Controlling growth and field emission property of aligned carbon nanotubes on porous silicon substrates, Appl. Phys. Lett. 75 (1999) 481–483, http://dx.doi.org/10.1063/1.124415.
[17] A. Gusain, N.J. Joshi, P.V. Varde, D.K. Aswala, Flexible NO gas sensor based on conducting polymer poly[N-9′-heptadecanyl-2,7-carbazole-alt-5,5-(4′,7′-di-2-thienyl-2′,1′,3′-benzothiadiazole)] (PCDTBT), Sens. Actuators B: Chem. 239 (2017) 734–745, http://dx.doi.org/10.1016/j.snb.2016.07.176.
[18] V.S. Angulakshmi, K. Rajasekar, C. Sathiskumar, S. Karthikeyan, Growth of vertically aligned carbon nanotubes on a silicon substrate by a spray pyrolysis method, New. Carbon Mater. 28 (2013) 284–287, http://dx.doi.org/10.1016/j.carbon.2013.07.075.
[19] R.A. Afre, T. Soga, T. Jimbo, M. Kumar, Y. Ando, M. Sharon, Growth of vertically aligned carbon nanotubes on silicon and quartz substrate by spray pyrolysis of a natural precursor: turpentine oil, Chem. Phys. Lett. 414 (2005) 6–10, http://dx.doi.org/10.1016/j.cplett.2005.08.040.
[20] Alireza Nikfarjam, Azam Iraji zad, Fatemeh Razi, S. Zahra Mortazavi, Fabrication of gas ionization sensor using carbon nanotube arrays grown on porous silicon substrate, Sens. Actuators A 162 (2010) 24–28, http://dx.doi.org/10.1016/j.sna.2010.06.015.
[21] N. Hordy, N.Y. Mendoza-Gonzalez, S. Coulombe, J.-L. Meunier, The effect of carbon input on the morphology and attachment of carbon nanotubes grown directly from stainless steel, Carbon 63 (2013) 348–357, http://dx.doi.org/10.1016/j.carbon.2013.06.089.
[22] V.E. Kan, V.V. Bolotov, K.E. Ivleva, E.V. Knyazev, V.E. Roslikov, Synthesis of the 'Carbon nanotubes-porous silicon' hybrid material for gas sensors, Procedia Eng. 152 (2016) 706–710, http://dx.doi.org/10.1016/j.proeng.2016.07.677.
[23] Y. Wang, J.T.W. Yeow, A review of carbon nanotubes-based gas sensors, J. Sens. (2009) (2009) 493904, http://dx.doi.org/10.1155/2009/493904.
[24] M.-B. Gholivand, A. Akbari, a novel and high sensitive MWCNTs-nickel carbide/hollow fiber-pencil graphite modified electrode for in situ ultra-trace analysis of bisphenol A, J. Electroanalyt. Chem. 817 (2018) 9–17, http://dx.doi.org/10.1016/j.jelechem.2018.03.065.
[25] X.C. Lu, L. Song, T.T. Ding, Y.L. Lin, C.X. Xu, CuS–MWCNT based electrochemical sensor for sensitive detection of bisphenol A, Russ. J. Electrochem. 53 (2017) 366–373, http://dx.doi.org/10.1134/S1023193517040073.
[26] Aneta Fraczek-Szczypta, Elzbieta Menaszek, Tahmina Bahar Syeda, Anil Misra, Mohammad Alavijeh, Jimi Adu, Stanislaw Blazewicz, Effect of MWCNT surface and chemical modification on in vitro cellular response, J. Nanopart. Res. 14 (2012) 1181, http://dx.doi.org/10.1007/s11051-012-1181-1.
[27] I. Khan, U.J. Pandit, S. Wankar, S.N. Limaye, Design of electrochemical sensor based on fMWCNT-CPE decorated with Ti nanofilm and its electrocatalytic behavior towards aminotriazole, Electrocatalysis 8 (2017) 196, http://dx.doi.org/10.1007/s12678-017-0358-x.
[28] V.M. Aroutiounian, Porous silicon gas sensors, in: R. Jaaniso, O.K. Tan (Eds.), Semiconductor Gas Sensors, Woodhead Publishing, 2013, http://dx.doi.org/10.1533/9780857098665.3.408.
[29] V.M. Aroutiounian, Gas sensors based on functionalized carbon nanotubes, J. Contemp. Phys. (Armen. Acad. Sci.) 50 (2015) 333–354, http://dx.doi.org/10.3103/S1068337215040064.
[30] L. De Luca, A. Donato, G. Apa, S. Santangelo, G. Faggio, G. Messina, N. Donato, A. Bonavita, G. Neri, Room temperature hydrogen sensor based on Pt/TiO_2/MWCNT composites, in: G. Neri, N. Donato, A. d'Amico, C. Di Natale (Eds.), Sensors and Microsystems, Springer, Netherlands, 2011, pp. 87–91.
[31] V.M. Arakelyan, M.S. Aleksanyan, R.V. Hovhannisyan, G.E. Shahnazaryan, V.M. Aroutiounian, K. Hernadi, Z. Nemeth, L. Forro, Gas sensors made of multiwall carbon nanotubes modified by tin dioxide, J. Contemp. Phys. (Armen. Acad. Sci.) 48 (2013) 176, http://dx.doi.org/10.3103/S1068337213040063.
[32] M. Penza, P.J. Martin, J.T.W. Yeow, Carbon nanotube gas sensors, in: C.-D. Kohl, T. Wagner (Eds.), Gas Sensing Fundamentals. Springer Series on Chemical Sensors and Biosensors (Methods and Applications), vol. 15, Springer, Berlin, 2014, pp. 109–174, http://dx.doi.org/10.1007/5346_2014_59.
[33] L.B. Kong, H. Huang, Thin film gas sensors based on nanocarbon materials, in: S. Li, J. Wu, Z. Wang, Y. Jiang (Eds.), Nanoscale Sensors. Lecture Notes in Nanoscale Science and Technology, vol. 19, Springer, Cham, 2013, pp. 189–223, http://dx.doi.org/10.1007/978-3-319-02772-2_7.
[34] Y.J. Kwon, A. Mirzaei, S.Y. Kang, M.S. Choi, J.H. Bang, S.S. Kim, H.W. Kim, Synthesis, characterization and gas sensing properties of ZnO-decorated MWCNTs, Appl. Surf. Sci. 413 (2017) 242–250, http://dx.doi.org/10.1016/j.apsusc.2017.03.290.
[35] S.Y. Hong, J.H. Oh, H. Park, J.Y. Yun, S.W. Jin, L. Sun, G. Zi, J.S. Ha, Polyurethane foam coated with a multi-walled carbon nanotube/polyaniline nanocomposite for a skin-like stretchable array of multi-functional sensors, NPG Asia Mater. 9 (2017) e448, http://dx.doi.org/10.1038/am.2017.194.
[37] S. Manivannan, J.H. Ryu, H.E. Lim, M. Nakamoto, J. Jang, K.C. Park, Properties of surface treated transparent conducting single walled carbon nanotube films, J. Mater. Sci: Mater. Electron. 21 (2010) 72–77, http://dx.doi.org/10.1007/s10854-009-9872-9.
[38] G. Santamaría-Juárez, E. Gómez-Barojas, E. Quiroga-González, E. Sánchez-Mora, J.A. Luna-López, Oxidized porous silicon as a non-interfering support for luminescent dyes, Mesoporous Biomater. 3 (2016) 61–66, http://dx.doi.org/10.1515/mesbi-2016-0008.

[39] M.C. Arenas, M. Vega, O. Martinez, O.H. Salinas, Nanocrystalline porous silicon: structural, optical, electrical and photovoltaic properties, in: S. Basu (Ed.), Crystalline Silicon - Properties and Uses, Intech, India, 2011, pp. 251–275.
[40] T.Z. Al-Tayyar, N.A. Salman, Impact of the variability in the current density on the porous silicon characteristics, Energy Procedia 50 (2014) 488–493, http://dx.doi.org/10.1016/j.egypro.2014.06.059.
[42] B. Gelloz, Photoluminescence of porous silicon, in: Leigh Canham (Ed.), Handbook of Porous Silicon, Springer, Switzerland, 2014, pp. 307–320, http://dx.doi.org/10.1007/978-3-319-05744-6_32.
[43] I.B. Olenych, Olenal. Aksimenyeva, L.S. Monastyrskii, Y.H. Horbenko, L.I. Yarystska, Sensory properties of hybrid composites based on poly (3,4-ethylenedioxythiophene)-porous silicon-carbon nanotubes, Nanoscale Res. Lett. 10 (2015) 1–6, http://dx.doi.org/10.1186/s11671-015-0896-1.
[44] G.M. Youssef, M.M. El-Nahass, S.Y. El-Zaiat, M.A. Farag, Investigation of size and band gap distributions of Si nanoparticles from morphology and optical properties of porous silicon layers formed on a textured N+ P silicon solar cell, Int. J. Semicond. Sci. Technol. 6 (2016) 1–12.
[45] H.J. Xu, X.J. Li, Silicon nanoporous pillar array: a silicon hierarchical structure with high light absorption and triple-band photoluminescence, Opt. Express 16 (2008) 2933–2941, http://dx.doi.org/10.1364/OE.16.002933.
[46] O. Bisi, S. Ossicini, L. Pavesi, Porous silicon: a quantum sponge structure for silicon based optoelectronics, Surf. Sci. Rep. 38 (2000) 1–126, http://dx.doi.org/10.1016/S0167-5729(99)00012-6.
[47] S.K. Ram, Electrical transport in porous silicon, in: Leigh Canham (Ed.), Handbook of Porous Silicon, Springer International Publishing, Switzerland, 2014, pp. 263–279, http://dx.doi.org/10.1007/978-3-319-05744-6_28.
[48] O.Ya. Olikh, Review and test of methods for determination of the schottky diode parameters, J. Appl. Phys. 118 (2015) 024502, http://dx.doi.org/10.1063/1.4926420.
[49] S.K. Cheung, N.W. Cheung, Extraction of schottky diode parameters from forward current-voltage characteristics, Appl. Phys. Lett. 49 (1986) 85–87, http://dx.doi.org/10.1063/1.97359.
[50] N.M. Triet, L.T. Duy, B.-U. Hwang, A. Hanif, S. Siddiqui, K.H. Park, C.-Y. Cho, N.-E. Lee, High-performance schottky diode gas sensor based on heterojunction of three-dimensional nanohybrids of reduced graphene oxide–vertical ZnO nanorods on AlGaN/GaN layer, ACS Appl. Mater. Interfaces 9 (2017) 30722–30732, http://dx.doi.org/10.1021/acsami.7b06461.
[51] L. Talazac, F. Barbarin, C. Varenne, L. Mazet, S. Pellier, C. Soulier, Gas sensing properties of pseudo-schottky diodes on p-type indium phosphide substrates: application to O_3 and NO_2 monitoring in urban ambient air, Sens. Actuators B: Chem. 83 (2002) 149–159, http://dx.doi.org/10.1016/S0925-4005(01)01055-3.
[52] Y. Fang, M. Akbari, J.G.D. Hester, L. Sydänheimo, L. Ukkonen, M.M. Tentzeris, Sensitivity enhancement of flexible gas sensors via conversion of inkjet-printed silver electrodes into porous gold counterparts, Sci. Rep. 7 (2017) 8988, http://dx.doi.org/10.1038/s41598-017-09174-5.
[53] L. Chandra, P.K. Sahu, R. Dwivedi, V.N. Mishra, Optimized hydrogen sensing characteristic of Pd/ZnO nanoparticles based schottky diode on glass substrate, Mater. Res. Express 4 (2017) 10, http://dx.doi.org/10.1088/2053-1591/aa8bc1.
[54] C. Peng, K.D. Hirschman, P.M. Fauchet, Carrier transport in porous silicon light-emitting devices, J. Appl. Phys. 80 (1996) 295, http://dx.doi.org/10.1063/1.362783.
[55] T.A. Burr, A.A. Seraphin, E. Werwa, K.D. Kolenbrander, Carrier transport in thin films of silicon nanoparticles, Phys. Rev. B 56 (1997) 4818–4824.
[56] S.M. Lyth, S.R.P. Silva, Electron Field emission from Water-based carbon nanotube inks, ECS J. Solid State Sci. Technol. 4 (2015) P3034–P3043, http://dx.doi.org/10.1149/2.0051504jss.
[57] R.C. Smith, D.C. Cox, S.R.P. Silva, Electron field emission from a single carbon nanotube: effects of anode location, Appl. Phys. Lett. 87 (2005) 103112, http://dx.doi.org/10.1063/1.2041824.
[58] G.S. Bocharov, A.V. Eletskii, Theory of carbon nanotube (CNT)-based electron field emitters, Nanomaterials 3 (2013) 393–442, http://dx.doi.org/10.3390/nano3030393.

Biographies

Natanael Victoriano Huerta was born in Puebla, Mexico, in 1987. He received the Master's degree in semiconductors in 2017 in the Instituto de Ciencias (Centro de Investigaciones en Dispositivos Semiconductores, IC-CIDS) from Benemérita Universidad Autónoma de Puebla. His thesis topic was Optical and electrical properties of porous silicon and porous silicon with carbon nanotubes deposited by spin coating.

J. A. Luna López was born in Veracruz, Mexico, in 1966. He obtained a PhD on Electronics at National Institute of Astrophysics, Optics and Electronics (INAOE), Mexico in 2007. He has two postdoctoral stays, in Center Nanoscience's and Nanotechnology of Mexico National Autonomous University of Mexico (CNN-UNAM) and in Benemérita Universidad Autónoma de Puebla (BUAP). He is currently a researcher and professor in the Institute of Science (Instituto de Ciencias-Centro de Investigaciones en Dispositivos Semiconductores, IC-CIDS) from BUAP, Puebla, México. He has been working on structural, electrical, and optical characterization of nanostructure materials (SRO, PSi, Phthalocyanines, CNTs, TCO, etc.) and different structures as MOS, M–S, TFT, Shottky barrers, etc. His research interest is the physics and technology of material nanostructures with nanocrystals (organic and inorganic) and optoelectronics devices. Additionally, his research interests are nanotechnology, material characterization, and photonics devices such as sensor, LEDs, and solar cells.

A.D. Hernández de la Luz was born in Puebla, Mexico, in1963. Is currently a researcher and professor in the Instituto de Ciencias (Centro de Investigaciones en Dispositivos Semiconductores, IC-CIDS) from Benemérita Universidad Autónoma de Puebla, México. He has been working on optical properties of semiconductors in the framework of local and nonlocal theory, Casimir forces with dispersive spatial effects and luminescent effects in compound semiconductors. Recently, his research interest is focused on electrical transport and luminescent properties of graphene and carbon nanotubes, also in electrical properties of the field effect transistor with channel of carbon nanotubes.

Estela Gómez Barojas was born in Puebla, México in 1949. She received the B.Sc and M.Sc degrees in Physics from Universidad Autónoma de Puebla in 1979 and 1983, respectively. She received the Ph. D. degree in Natural science from Ludwig-Maximilian University, Munich, Germany in 1990. She is working at the Institute of Science, Universidad Autónoma de Puebla and her current research topic is in Porous Silicon.

Karim Monfil Leyva was born in Veracruz, Mexico, in 1975. He obtained a PhD on Electronics at National Institute of Astrophysics, Optics and Electronics (INAOE), Mexico in 2009. He has two postdoctoral stays, in Autonomous University of Juarez City (UACJ) and in Mexico National Autonomous University of Mexico (UNAM). He is a Titular Professor Researcher at Meritorious Autonomous University of Puebla (BUAP), since 2012. He is a member of the Materials Research Society and author or reviewer of Elsevier Journals. He has a wide knowledge on thin film deposition techniques and optical and electrical characterization.

Miguel A. Dominguez was born in Veracruz, Mexico, in 1981. He received the B.Sc. degree from Veracruz Institute of Technology, Mexico, in 2004 and the M.Sc. and pH.D. degrees from the National Institute for Astrophysics, Optics and Electronics (INAOE), Mexico, in 2008 and 2012, respectively. In 2012, he joined the University of Texas at Dallas, USA, Department of Materials Science and Engineering. Since 2014, he is with Centro de Investigaciones en Dispositivos Semiconductores, Benemerita Universidad Autonoma de Puebla (BUAP), Mexico.